Numerical computation of coherent structures

Alan R. Champneys[1] and Björn Sandstede[2]

[1] Department of Engineering Mathematics, University of Bristol, United Kingdom
[2] Department of Mathematics, University of Surrey, United Kingdom

In many applications one is interested in finding solutions to nonlinear evolution equations with a particular spatial and temporal structure. For instance, solitons in optical fibers and wave guides or buckling modes of long structures can be interpreted as localised travelling or standing waves of an appropriate underlying partial differential equation (PDE) posed on an unbounded domain. Spiral waves or other defects in oscillatory media are time-periodic waves with an asymptotic spatially periodic structure. All of these examples are referred to as *coherent structure*. They represent relative equilibria, that is, their temporal evolution is determined by a symmetry of the underlying PDE: namely, translational symmetry for travelling waves, rotational symmetry for spiral waves, and phase symmetry for oscillatory structures.

Given the complexity of typical PDE models, these nonlinear waves are in general accessible only through numerical computations. One possible approach is via direct simulation which is, however, expensive and fails to capture solutions that are either unstable or may have a small basin of stability. Simulation also fails to provide valuable information on how branches of solutions are organised in parameter space.

In this chapter, we give an overview of boundary-value problem formulations for coherent structures which provide a robust and less expensive alternative to simulation. Moreover, setting up well-posed boundary-value problems allows us to continue solutions in parameters space, investigate their spectral stability directly, and continue branches of solutions efficiently as parameters vary.

In the next section we outline how PDEs can be supplemented by phase conditions that allow us to compute nonlinear waves as regular zeros of the resulting nonlinear system. In the remaining sections, we treat different kinds of coherent structures, namely travelling waves, time-periodic structures, and planar localised patterns. In each case we explain how to set up a well-posed boundary-value problem and illustrate the theory with the results of an example computation.

1 Symmetries and phase conditions

It is desirable to formulate the problem of computing nonlinear waves in such a way that solutions correspond to regular zeros of an appropriate smooth function. Indeed, Newton's method is then applicable and gives a robust and efficient way of computing zeros. When computing coherent structures, solutions are often not unique due to the presence of translational or other symmetries in the underlying partial differential equation. In other words, symmetries may give rise to families of solutions. To make Newton's method work, we need to single out one particular solution. This can be done by adding extra functionals to the problem and identifying additional parameters that compensate for the added functional to make the overall problem invertible; see also Chapters 9 and 10. In this section, we recall how the extra functionals, which we refer to as phase conditions, can be constructed and the additional parameters be identified in systems with symmetries.

Thus, consider the equation

$$u_t = f(u), \qquad u \in \mathcal{X} \tag{1}$$

where $\mathcal{X}$ is a Banach space. For ease of exposition, we assume that $f : \mathcal{X} \to \mathcal{X}$ is smooth; we remark that this assumption does not hold if (1) represents a partial differential equation, but the results that follow actually hold for PDEs nevertheless.

The key assumption is that (1) is equivariant under the action of a finite-dimensional Lie group G on $\mathcal{X}$ so that

$$gf(u) = f(gu), \qquad \forall g \in G,\ \forall u \in \mathcal{X}.$$

We denote by

$$\exp : \mathrm{alg}(G) \longrightarrow G, \quad \xi \longmapsto \exp(\xi)$$

the exponential map of the Lie algebra $\mathrm{alg}(G)$ of G into G.

Example 1. Take $\mathcal{X} = C^1(\mathbb{R}, \mathbb{R}^n)$ and consider the action of $G = \mathbb{R}$ defined by $g : \mathcal{X} \to \mathcal{X}$, $u(\cdot) \mapsto u(\cdot + g)$ for all $g \in G = \mathbb{R}$; then $\exp = \mathrm{id}$.

Particularly interesting solutions $u(t)$ of (1) are relative equilibria which are equilibria when the group action is factored out. More precisely, u_* is a relative equilibrium if there exists $\xi_* \in \mathrm{alg}(G)$ so that

$$u(t) = \exp(\xi_* t)u_* \qquad \forall t \in \mathbb{R}.$$

Note that $u(t) \in Gu_*$ for all t. We emphasize that u_* satisfies

$$\xi_* u_* = f(u_*) \tag{2}$$

where we identify an element $\xi \in \mathrm{alg}(G)$ with the generator

$$\xi = \frac{\mathrm{d}}{\mathrm{d}t} \exp(\xi t)\Big|_{t=0} : \mathcal{X} \longrightarrow \mathcal{X}$$

of the one-parameter group $\exp(\xi t)$.

Example 2 (Example 1 continued). Relative equilibria of the group action $g : \mathcal{X} \to \mathcal{X}$, $u(\cdot) \mapsto u(\cdot + g)$ for $g \in G = \mathbb{R}$ on $\mathcal{X} = C^1(\mathbb{R}, \mathbb{R}^n)$ are of the form $u(x,t) = u_*(x + c_0 t)$ for $c_0 \in \mathbb{R}$. Therefore, they are travelling waves and we have

$$\xi_* u_* := \frac{\mathrm{d}}{\mathrm{d}t} \exp(c_0 t) u_*\Big|_{t=0} = \frac{\mathrm{d}}{\mathrm{d}t} u_*(\cdot + c_0 t)\Big|_{t=0} = u_*'(\cdot + c_0 t)\Big|_{t=0} = c_0 u_*',$$

and (2) becomes the travelling wave equation $c_0 u_*' = f(u_*)$.

If u_* is a relative equilibrium then the entire group orbit Gu_* consists of relative equilibria since

$$gu(t) = g \exp(\xi_* t) g^{-1} g u_* = \exp(\mathrm{Ad}_g \xi_* t) g u_*$$

is again a relative equilibrium, where

$$\mathrm{Ad}_g \xi := \frac{\mathrm{d}}{\mathrm{d}t} g \exp(\xi t) g^{-1}\Big|_{t=0} \in \mathrm{alg}(G).$$

If G is Abelian, then Ad_g is the identity, and the velocity ξ_* is the same for all relative equilibria in the group orbit Gu_*.

Example 3 (Example 1 continued). With $u(t) = u_*(\cdot + c_0 t)$, we find that $u_*(\cdot + g + c_0 t)$ is a travelling wave for each $g \in G = \mathbb{R}$.

Thus, to compute or continue relative equilibria, we need to solve

$$f(u) - \xi u = 0$$

for $(u, \xi) \in \mathcal{X} \times \mathrm{alg}(G)$ and expect to find a family $\{(gu_*, \mathrm{Ad}_g \xi_*);\ g \in G\}$ of solutions. To find (u, ξ) as a regular zero of an appropriate function, we need to add phase conditions that single out a relative equilibrium (u_*, ξ_*) among the family of solutions.

For simplicity, we assume from now on that the Lie group G is Abelian. The family of relative equilibria is then given by (gu_*, ξ_*) for $g \in G$, and we have $f(gu_*) - \xi_* g u_* = 0$ for all $g \in G$. Choosing $g = \exp(\xi t)$ and taking the derivative with respect to t at $t = 0$, we obtain

$$f_u(u_*)\xi u_* - \xi_* \xi u_* = 0$$

for all $\xi \in \mathrm{alg}(G)$. Thus, if we assume that the isotropy group $\{g \in G;\ gu_* = u_*\}$ is discrete, we can conclude that the linearisation $f_u(u_*) - \xi_*$ of (2) has a null space of dimension at least $\dim G$ with elements ξu_* for $\xi \in \mathrm{alg}(G)$.

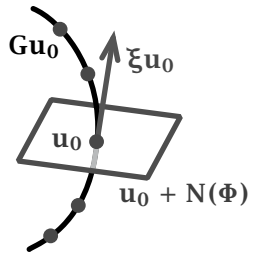

Fig. 1. The translated null space $u_* + \mathrm{N}(\Phi)$ of an admissible phase condition is transverse to the group orbit Gu_* at the relative equilibrium u_*. Imposing the condition $\Phi(u - u_*) = 0$ restricts u to $u_* + \mathrm{N}(\Phi)$ and, therefore, singles out the relative equilibrium u_*.

Hypothesis 1 *Assume that G is Abelian with $\dim G = m$, and (u_*, ξ_*) is a relative equilibrium such that $f_u(u_*) - \xi_*$ is a Fredholm operator with index zero. Furthermore, assume that $f_u(u_*) - \xi_*$ has an eigenvalue $\lambda = 0$ with geometric and algebraic multiplicity m and that its null space is given by $\{\xi u_*\}_{\xi \in \mathrm{alg}(G)}$.*

We choose linear phase conditions of the form

$$\Phi : \mathcal{X} \longrightarrow \mathbb{R}^m, \quad u \longmapsto \Phi u$$

and say that Φ is admissible if the linear operator

$$\mathrm{alg}(G) \longrightarrow \mathbb{R}^m, \qquad \xi \longmapsto \Phi \xi u_*$$

is invertible.

Theorem 1. *Assume that Hypothesis 1 holds and that Φ is an admissible phase condition. Then the relative equilibrium (u_*, ξ_*) is a regular zero of the map*

$$\mathcal{F} : \mathcal{X} \times \mathrm{alg}(G) \longrightarrow \mathcal{X} \times \mathbb{R}^m, \quad (u, \xi) \longmapsto (f(u) - \xi u, \Phi(u - u_*)).$$

Proof. Clearly, $\mathcal{F}(u_*, \xi_*) = 0$. The linearisation of $\mathcal{F}$ about (u_*, ξ_*) is given by

$$\mathcal{L} : (u, \xi) \longmapsto ([f_u(u_*) - \xi_*]u - \xi u_*, \Phi u).$$

The bordering lemma [3, Lemma 2.3] shows that this operator is Fredholm with index zero and, therefore, it suffices to show that its null space is trivial. Since the geometric and algebraic multiplicities of the eigenvalue $\lambda = 0$ of $f_u(u_*) - \xi_*$ are equal to each other, there is a spectral decomposition

$$\mathcal{X} = \tilde{\mathcal{X}} \oplus \{\xi u_*;\ \xi \in \mathrm{alg}(G)\}$$

so that $f_u(u_*) - \xi_*$ is an isomorphism from $\tilde{\mathcal{X}}$ into itself. Writing $u = \tilde{u} + \zeta u_*$, we find

$$\mathcal{L}(u, \xi) = \mathcal{L}(\tilde{u} + \zeta u_*) = ([f_u(u_*) - \xi_*]\tilde{u} - \xi u_*, \Phi(\tilde{u} + \zeta u_*)).$$

Using again the decomposition of $\mathcal{X}$, we see that $\tilde{u} = \xi = 0$, and the remaining equation $\Phi \zeta u_* = 0$ finally gives $\zeta = 0$ since Φ is admissible. □

Remark 1. Suppose that $\mathcal{X}$ is a Hilbert space with scalar product $\langle \cdot, \cdot \rangle$ and choose a basis $\{\xi_j\}_{j=1,\ldots,m}$ of $\mathrm{alg}(G)$. Then the phase condition

$$\Phi : \mathcal{X} \longrightarrow \mathbb{R}^m, \quad u \longmapsto (\langle \xi_j u_*, u \rangle)_{j=1,\ldots,m}$$

is admissible.

Example 4 (Example 1 continued). We wish to find a functional $\Phi : C^1(\mathbb{R}, \mathbb{R}^n) \to \mathbb{R}$ such that $\Phi u_*' \neq 0$. The space $C^1(\mathbb{R}, \mathbb{R}^n)$ is not a Hilbert space, but if u_*' decays exponentially, then

$$\Phi u = \int_{\mathbb{R}} \langle u_*'(x), u(x) \rangle \, \mathrm{d}x$$

is an admissible phase condition.

2 Travelling waves: pulses and fronts

We consider systems of ordinary differential equations (ODEs) of the form

$$u_x = f(u; \alpha), \quad x \in \mathbb{R}, \quad u \in \mathbb{R}^n, \quad f \in C^1(\mathbb{R}, \mathbb{R}^n), \quad \alpha \in \mathbb{R}^p. \tag{3}$$

Such problems typically arise as steady state or travelling wave reductions of PDEs of the form

$$U_t = DU_{XX} + F(U; \beta), \qquad U \in \mathbb{R}^N.$$

Here, for a travelling wave $U(X, t) = U(X - ct)$ of speed c, we have $x = X - ct$, $u = (U, V) = (U, U_X)$, $\alpha = (c, \beta)$, and $f(u; \alpha) = (V, -D^{-1}[F(U; \beta) + cU])$.

Front solutions $q(x)$ of (3) at parameter values α_* correspond to heteroclinic connections between equilibria, and solve the following boundary-value problem on the real line

$$\begin{cases} q_x = f(q(x); \alpha_*) \\ q(x) \to u_0 \text{ as } x \to -\infty, \quad f(u_0; \alpha_*) = 0 \\ q(x) \to u_1 \text{ as } x \to \infty, \quad f(u_1; \alpha_*) = 0. \end{cases} \tag{4}$$

In the special case that $u_0 = u_1$, the pulse $q(x)$ corresponds to a homoclinic orbit of the ODE.

To set up a well-posed numerical boundary-value problem for solution of (4), we need to deal with the infinite interval $x \in (-\infty, \infty)$ in some way, to replace the asymptotic boundary conditions by some regular condition, and to deal with the translation symmetry $q(x) \to q(x+g)$. Several approaches for performing this task have been proposed, including shooting methods [25, 37], computation of large-period periodic orbits [39], and mapping the infinite domain to a finite interval; see, e.g., [26]. We focus here on methods, owing to Beyn [3] and Friedman & Doedel [15, 18], that involve truncation to a finite a domain $[-L, L]$ and use projection boundary conditions.

Suppose that the matrices $f_u(u_j; \alpha)$ have n_j^s eigenvalues (counting multiplicities) with negative real part, n_j^c eigenvalues with zero real part, and n_j^u eigenvalues with positive real part, so that $n_j^s + n_j^c + n_j^u = n$ for $j = 1, 2$. To set up a numerical boundary-value problem we then look for a solution $u(x)$ with $x \in [-L, L]$ subject to the boundary conditions

$$P^s(u_0; \alpha)(u(-L) - u_0) = 0, \qquad P^u(u_1; \alpha)(u(L) - u_1) = 0. \tag{5}$$

Here $P^s(u_0, \alpha)$ is an $n_0^s \times n$ matrix whose rows form a basis for the stable eigenspace of $f_u^T(u_0; \alpha)$. Accordingly, $P^u(u_1; \alpha)$ is an $n_1^u \times n$ matrix, whose rows form a basis for the unstable eigenspace of $f_u^T(u_1; \alpha)$. The boundary conditions (5) thus place the boundary points in the centre-unstable eigenspace of $f_u(u_0; \alpha)$ and centre-stable eigenspace of $f_u(u_1; \alpha)$, respectively.

If each of the equilibria u_j is hyperbolic, then $n_j^c = 0$, and by simply counting dimensions of the corresponding stable and unstable manifolds under generic hypotheses on transversality, we find that the codimension of the parameter set in which there exists a heteroclinic connection is equal to $m = n - (n_0^u + n_1^s) + 1$. If this number is negative then additional internal boundary conditions need to be set up to choose a member of the $|m|$-dimensional continuum of connections. From now on, we assume that m is non-negative. Hence, we need to free m parameters, say, $(\alpha_1, \ldots, \alpha_m)$ to find a regular solution to the boundary-value problem (3) and (5). However, (5) represents only

$$n_0^s + n_1^u = (n - n_0^u) + (n - n_1^s) = n + m$$

conditions for the $n + m + 1$ unknowns $u \in \mathbb{R}^n$ and $(\alpha_1, \ldots, \alpha_m)$, so that we need an extra condition. At the same time, we see that the original problem respects a translation symmetry since if $u(x)$ solves (4), then so does $u(x+g)$ for any $g \in \mathbb{R}$. So, according to the theory of Sec. 1, we need a phase condition that is transverse to the generator $\xi u = u_x$. Such a condition can be posed at a specific point in the domain, for example, at the left-hand boundary

$$\Phi(u) := \langle v, u(-L) \rangle = 0 \qquad \text{where } v \text{ is such that} \quad \langle v, u_x(-L) \rangle \neq 0. \tag{6}$$

This is equivalent to choosing the left-hand boundary point to be in the Poincaré section $\Sigma = \{u \in \mathbb{R}^n;\ \langle v, u \rangle = 0\}$, with the inner product condition

implying that the corresponding trajectory of (3) crosses Σ transversally. However, for practical implementation in continuation software, one cannot guarantee *a priori* that all solutions along a branch will remain transverse to Σ for all parameter values α. Therefore, it is better to take as phase condition the integral condition

$$\Phi(u) := \int_{-L}^{L} \langle u'_*(x), u(x) \rangle \, \mathrm{d}x \tag{7}$$

where u_* is a reference solution (for example the previously computed solution along a continuation branch); see also Chapters 1, 9 and 10.

Thus we solve the two-point boundary-value problem

$$\begin{pmatrix} u_x = f(u;\alpha) \\ P^s(u_0;\alpha)(u(-L) - u_0) \\ P^u(u_1;\alpha)(u(L) - u_1) \\ \int_{-L}^{L} \langle u'_*(x), u(x) - u_*(x) \rangle \, \mathrm{d}x \end{pmatrix} = 0. \tag{8}$$

Under certain non-degeneracy conditions, the existence of a homoclinic solution to the original problem (4) on the infinite interval implies the existence of a unique solution to the truncated problem (8) provided L is sufficiently large; see [18, 3, 38]. Furthermore, the error involved in the truncation scales exponentially with L for both the parameter and the solution.

There have been a number of implementations of the above algorithm for computing homoclinic and heteroclinic connections. For example, the routines HomCont [7] are part of the package Auto [14]. Some extensions to this basic algorithm allow one to deal with special situations as we now outline:

Reversibility

Many ODEs arise from reductions of even-order PDEs that contain only even spatial derivatives. In this case, the ODE can be written as an even-dimensional reversible system with respect to an involution $\mathcal{R}$ so that

$$f(\mathcal{R}u;\alpha) = -\mathcal{R}f(u;\alpha)$$

with $\mathcal{R}^2 = \mathrm{id}$ and $\dim \mathrm{Fix}(\mathcal{R}) = n/2$. Standing symmetric pulses, which are invariant under $x \mapsto -x$, correspond to reversible homoclinic orbits q to a reversible hyperbolic equilibrium u_0, and are of codimension-zero in parameter space [6, 12]. For a such an orbit we can replace the right-hand boundary condition of (5) by the condition $u(0) \in \mathrm{Fix}(\mathcal{R})$. Note that, provided the solution $q(x)$ intersects $\mathrm{Fix}(\mathcal{R})$ transversally, this boundary condition also breaks the translation invariance of the system. Therefore, there is no need for a phase condition. This is good since we require one condition less, which agrees with having one free parameter less compared to the non-reversible case. This approach has been used extensively to compute so-called *gap solitons* in nonlinear optics; see e.g. [11].

Hamiltonian systems

Muñoz-Almaraz *et al.* [33] consider how to compute periodic orbits in Hamiltonian systems; see also Chapter 9. Their approach naturally extends to heteroclinic connections under generic hypotheses on the connection. Hamiltonian systems conserve a first integral, the Hamiltonian itself. Noether's theorem says that any other independent (in the sense of a Poisson bracket) conserved quantity $\mathcal{C}(u)$ corresponds to a symmetry of the underlying system. Thus each conserved quantity (including the Hamiltonian) reduces the codimension of the solution one is trying to compute. Thus we need to remove one boundary condition for each additional conserved integral, or introduce an extra artificial parameter. The approach used in [33], for a system which k independent conserved smooth scalar functionals $\mathcal{C}_j : \mathbb{R}^n \times \mathbb{R}^p \to \mathbb{R}$ for $j = 1, \ldots, k$, is to introduce artificial parameters $\tilde{\alpha} \in \mathbb{R}^k$ and solve

$$u_x = f(u;\alpha) + \sum_{j=1}^{k} \tilde{\alpha}_j \partial_u \mathcal{C}_j(u;\alpha). \tag{9}$$

It has been proved rigorously that this leads to well-posed boundary-value problems under appropriate generic hypotheses. Importantly, $\tilde{\alpha} = 0$ for the true solution to the boundary-value problem and that $\partial_u \mathcal{C}_j(u;\alpha)$ is precisely orthogonal to the level set of $\mathcal{C}_j$, which is in keeping with the theory of Sec. 1 above. Note that we still need to retain exactly the same projection boundary conditions (5) and (7), but now the free parameters are replaced with the artificial parameters $\tilde{\alpha} \in \mathbb{R}^k$.

Non-hyperbolic equilibria

If $u_0 = u_1$ is a non-hyperbolic equilibrium, then one has to make special considerations to determine the codimension of the homoclinic connection and, hence, the number of free parameters that is needed. We consider two cases separately.

Our first case of interest is that when $u_0 = u_1$ and $n^c = 2$ with a pair of pure imaginary eigenvalues in the spectrum. In Hamiltonian or reversible systems such a linearisation is generic, and such points are called saddle-centres if $n^u = n^s > 0$: in this situation, it is then possible to form homoclinic connections with exponentially decaying tails that lie in the stable and unstable manifolds of the equilibrium. Such solutions in reversible systems correspond to so-called *embedded solitons* of nonlinear wave problems [45]. To compute these objects, we must replace the boundary condition (5) with

$$P^{cs}(u_0;\alpha)(u(-L) - u_0) = 0, \qquad u(0) \in \mathrm{Fix}(\mathcal{R})$$

where $P^{cs}(u_0;\alpha)$ is the spectral projection onto the centre-stable eigenspace of u_0 whose rows therefore form a basis for the centre-stable eigenspace of $f_u^T(u_0;\alpha)$.

The second case we consider is that $u_0 = u_1$ is a saddle node. Then pulse solutions can exist with algebraic decay as $x \to \pm\infty$. Besides the condition that u_0 is a saddle-node equilibrium, which can be taken to be $\det f_u(u_0;\alpha) = 0$, we provide the $n-1$ boundary conditions (5) plus the phase condition (7). In particular, these solutions have codimension one in the parameter space; see, e.g., [24, §7.1.2].

Saddle-homoclinic orbits and their orientation

Homoclinic bifurcations of various kinds can be treated by freeing an additional parameter α_j and adding appropriate conditions whose regular zeros define the extra degeneracy along a branch of homoclinic solutions; see [7] for a number of examples.

We discuss here a particular kind of codimension-two bifurcation that is known to lie at the heart of the creation of multi-pulse solutions from a branch of one-pulses, namely the so-called *inclination-flip* homoclinic bifurcation. It is caused by a degeneracy in the global twistedness of the stable and unstable manifolds $W^{s,u}(u_0)$ of a saddle u_0 around its homoclinic orbit $q(x)$; see e.g. [36] and references therein. At each point $q(x)$ along the homoclinic orbit, the normal bundle

$$Z(x) = [T_{q(x)}W^s(u_0) + T_{q(x)}W^u(u_0)]^\perp$$

of the tangent spaces of stable and unstable manifolds can be defined. Generically, these tangent spaces intersect along the one-dimensional subspace spanned by $q'(x)$ and, therefore, $Z(x)$ is one-dimensional for each x. The collection of $Z(x)$ generically forms a one-dimensional bundle along the set $\mathbb{S}^1 \cong \{u_0\} \cup \{q(x);\ x \in \mathbb{R}\}$ which can be orientable (homeomorphic to a cylinder) or non-orientable (homeomorphic to a Möbius band). Inclination-flips occur at codimension-two points in parameter space where this bundle changes from orientable to non-orientable (or vice versa). An efficient way to detect inclination-flip points is to compute normal vectors $w(x) \in Z(x)$ as solutions to the adjoint variational problem

$$w_x = -f_u^T(q(x);\alpha)w, \qquad w \to 0 \text{ as } x \to \pm\infty. \tag{10}$$

If we truncate, then we can approximate $w(x)$ on the same finite interval $[-L, L]$ as $q(x)$ by defining boundary conditions

$$Q^u(u_0;\alpha)w(-L) = 0, \qquad Q^s(u_1;\alpha)w(L) = 0, \tag{11}$$

where $Q^u(u_0;\alpha)$ is an $n^u \times n$ matrix whose rows form a basis for the unstable eigenspace of $f_u(u_0;\alpha)$. Similarly, $Q^s(u_1;\alpha)$ is an $n^s \times n$ matrix, whose rows form a basis for the stable eigenspace of $f_u(u_1;\alpha)$. Note that a solution to (10) is only defined up to scalar multiplication $w \to gw$. Therefore, we need a phase condition that fixes the amplitude which we may take to be

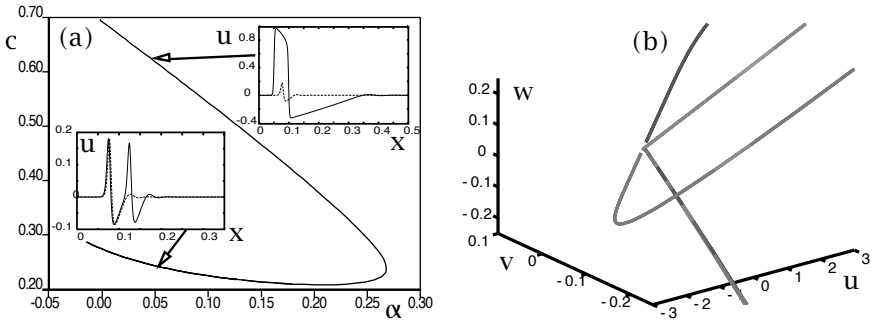

Fig. 2. Panel (a) shows a continuation of the branch of single-pulses to the FitzHugh–Nagumo system (15) for $\gamma = 0$ and $\varepsilon = 0.025$; the insets show the fast and the slow pulse for $\alpha = 0.02$ and a two-pulse orbit that is close to the slow pulse. Panel (b) is an enlargement near the origin of the solution of the adjoint variational equation around the pulse at the inclination-flip point and at two points that are parameter perturbations of $O(10^{-3})$ along the branch of homoclinic solutions.

$$\Phi(w) = \int_{-L}^{L} \langle w_*(x), w(x) - w_*(x) \rangle \, \mathrm{d}x = 0 \tag{12}$$

where $w_*(x)$ is a reference solution (for instance, the solution computed at a previous continuation step). Note though that (12) and (11) provides $n+1$ boundary conditions, so we need to free an additional parameter. In this case, it is convenient to include a parameter α_0 that unfolds the orthogonality of w and u_x:

$$w_x = -f_u^T(u(x);\alpha)w + \alpha_0 f(u(x);\alpha) \tag{13}$$

with the true solution to (13), (11), and (12) satisfying $\alpha_0 = 0$ as $w \to 0$.

We finish with an example, namely the FitzHugh–Nagumo system; see also [14] for a demo on switching branches to multi-pulse orbits in this system, during continuation of a single pulse, and also for references. It is given by the PDE

$$\begin{aligned} u_t &= u_{yy} - f_\alpha(u) - w, \qquad f_\alpha(u) = u(u-\alpha)(u-1) \\ w_t &= \varepsilon(u - \gamma w). \end{aligned} \tag{14}$$

for the functions $(u, w)(y, t)$. Looking for travelling waves by letting $x = y + ct$, we obtain the ODE system

$$\begin{aligned} u_x &= v \\ v_x &= cv + f_\alpha(u) + w \\ w_x &= \frac{\varepsilon}{\gamma}(u - \gamma w). \end{aligned} \tag{15}$$

Figure 2 shows the result of numerical continuation of the single pulse solution in the (α, c)-plane for $\gamma = 0$ and $\varepsilon = 0.025$. Note that for most

values of α there are either none or two wave speeds c for which there exists a travelling pulse. The faster wave is the one that is generally stable. Note that both the upper and the lower branch appear to end 'in mid air' as α is reduced. In fact, the branches fold back on themselves and the pulses return as their own two-pulse orbits at very nearby parameter values to those at which the one-pulse exists; see the dashed curve in the inset to Fig. 2(a).

For α sufficiently large ($\alpha > 0.1318124$ on the lower branch and $\alpha > 0.107652$ on the upper branch) the tail of the pulse has monotonic decay because the origin of the ODE system (15) is a real saddle. In such circumstances, the orientability of the normal bundle to the stable and unstable manifolds along the homoclinic orbit is well-defined. Indeed we find that at $(\alpha, c) = (0.240314, 0.211443)$ there is an inclination flip with respect to the stable manifold; see Fig. 2(b). Theoretical and numerical work for inclination flips in the FitzHugh–Nagumo system can also be found in [23].

3 Travelling waves with spatially periodic asymptotics

Dieci & Rebaza [13] considered a general boundary-value approach for computing heteroclinic connections between hyperbolic periodic orbits and from equilibria to periodic orbits for ODEs. These correspond to travelling waves whose profile becomes spatially periodic as $x \to \infty$ and/or $x \to -\infty$. For the special case where the periodic solutions in the two tails are the same (up to a phase shift), a popular approach for computing such generalised pulses is to study the problem in the setting of a Poincaré map and to compute homoclinic connections to hyperbolic fixed points of the map; see, for example, [5, 1, 21] and also the AUTO implementation HOMMAP due to Yagasaki [44]. Instead, we present here the approach from [13] (see also [22]) that relies on setting up a coupled boundary-value problem for the periodic orbits and the homoclinic orbit.

Suppose a connection $q(x)$ is sought between two separate hyperbolic periodic solutions $p_j(x;\alpha)$ with periods L_j for $j = 0, 1$ which have n_j^s Floquet multipliers inside the unit circle and $n_j^u = n - n_j^s + 1$ outside. Note that $n_j^c = 1$ due to the presence of the trivial Floquet multiplier 1. We then seek a solution to the boundary-value problem

$$\begin{pmatrix} u' - f(x;\alpha) \\ v_{0,1}' - f(v^{0,1};\alpha) \\ v_{0,1}(0) - v_{0,1}(L_{0,1}) \\ P^{cs}(v_0;\alpha)(u(-L) - v_0(0)) \\ P^{cu}(v_1;\alpha)(u(L) - v_1(0)) \\ \Phi_{0,1}(v_{0,1} - v_{0,1}^*) \end{pmatrix} = 0 \tag{16}$$

with solution (u, v_0, v_1) near (q, p_0, p_1). Here, the projection boundary condition $P^{cs}(v_0;\alpha)$ is an $(n_0^s + 1) \times n$ matrix whose columns are orthogonal

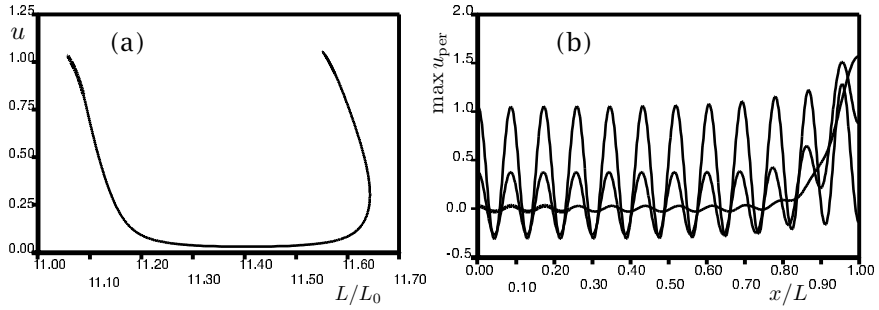

Fig. 3. Homoclinic orbits to periodic orbits of (17) computed on the half-interval $[-L, 0]$ (a), and their locus in the phase-shift versus tail amplitude plain (b). Reproduced from A.R. Champneys and G.J. Lord, Computation of homoclinic solutions to periodic orbits in a reduced water-wave problem, *Physica D*, 102 (1997) 101–124 © 1997, with permission from Elsevier Science.

to the unstable eigenspace of the monodromy matrix associated with v_0 at $x = 0$. In other words, the rows of $P^{cs}(v_0; \alpha)$ are formed by the centre-stable Floquet eigenspace of the adjoint variational problem $w_x = f_u^T(v_0(x); \alpha)w$ for $x \in [0, L_0]$. Note the importance of solving the *adjoint* problem in order that the projection represented by P^{cs} is orthogonal to the unstable Floquet eigenspace, rather than being along the centre-stable Floquet directions (this detail was inadvertently omitted in [13]). Similarly, P^{cu} sets the component orthogonal to the stable Floquet eigenspace to zero. The phase conditions $\Phi_{0,1}$ are chosen to factor out the translation symmetry of the periodic orbits, and may be taken to be

$$\Phi_j(v) = \int_0^{L_j} \langle \partial_x v_j^*(x), v(x) \rangle \, \mathrm{d}x, \qquad j = 1, 2,$$

where $v_j^*(x)$ are reference periodic solutions (we may again take v_j^* to be p_j computed at a precious point along a continuation branch). Note that there is no phase condition on the heteroclinic orbit $u(x)$ since the translation symmetry is broken by fixing the phase of the two periodic orbits. Moreover, the intervals L_0, L_1 and L should all be taken as unknowns. This is because L_0 and L_1 are the *a priori* unknown periods of the periodic orbits p_0 and p_1, and L must be taken to be free in order to solve the unknown *phase shift* between the periodic orbits p_0 and p_1.

Practical implementation details of the boundary-value problem (16) are discussed in [13], which also contains a convergence proof based on the methods of [4]. In particular, care has to be taken in order to evaluate the matrices $P^{cs}(v_0; \alpha)$ and $P^{cu}(v_1; \alpha)$ which themselves depend on the solutions $v_j(x)$.

We illustrate the approach outlined above by considering an application to a fourth-order water-wave problem. Champneys & Lord [9] consider the system

$$\varepsilon^2 u^{iv}(x) + u''(x) - u(x) + u(x)^2 = 0, \quad x \in \mathbb{R}, \tag{17}$$

where $u(x)$ represents the amplitude of water waves in the presence of surface tension for a model equation that is only valid for small-amplitude waves close to the critical point of Bond number 1/3 and Froude number 1. Equation (17) can easily be shown to be equivalent to a fourth-order Hamiltonian system, with total energy given by

$$\mathcal{H} = \varepsilon^2 u' u''' + \frac{[u']^2}{2} - \frac{\varepsilon^2}{2}[u'']^2 - \frac{u^2}{2} + \frac{u^3}{3}.$$

The problem is also reversible with respect to the involution

$$\mathcal{R}: \quad (u, u', u'', u''') \longrightarrow (u, -u', u'', -u''').$$

Figure 3 shows the results of computations of reversible homoclinic orbits to reversible periodic orbits, where the right-hand boundary conditions in (16) are replaced with $u(0) \in \mathrm{Fix}(\mathcal{R})$ and $v_0(L_0/2) \in \mathrm{Fix}(\mathcal{R})$.

Similar results were found for the full water-wave problem in the presence of surface tension using boundary-integral methods [10]; see Fig. 4. These careful computations helped to settle a conjecture (in the negative) of whether true solitary waves of elevation exist in the classical water wave problem; see also [40].

4 Moving discrete breathers in $\mathbb{R} \times \mathbb{Z}$

The discrete nonlinear Schrödinger equation (DNLS) with a saturable nonlinear term, representing the effects of a photorefractive crystal lattice, may be written in the form

$$\mathrm{i}\dot{u}_n(t) = -\varepsilon[\Delta_2 u(t)]_n + \frac{u_n(t)}{1 + |u_n(t)|^2}, \quad n \in \mathbb{Z} \tag{18}$$

where Δ_2 is the standard second-order spatial difference operator $[\Delta_2 u]_n = u_{n+1} - 2u_n + u_{n-1}$, and ε represents the dimensionless coupling strength between each lattice site. Localised time-periodic solutions to such equations have been given the name *discrete breathers*.

Standing discrete breathers are relatively easy to compute since, after making a phase transformation $u_n(t) = \mathrm{e}^{\mathrm{i}\Lambda t} U_n$, one has to solve for homoclinic orbits of the discrete map

$$\mathrm{i}\Lambda U_n = -\varepsilon[\Delta_2 U]_n + \frac{U_n}{1 + |U_n|^2}, \quad n \in \mathbb{Z},$$

which are structurally stable (and indeed many of which are stable and may be found as solutions of the initial-value problem (18)). However, if one tries

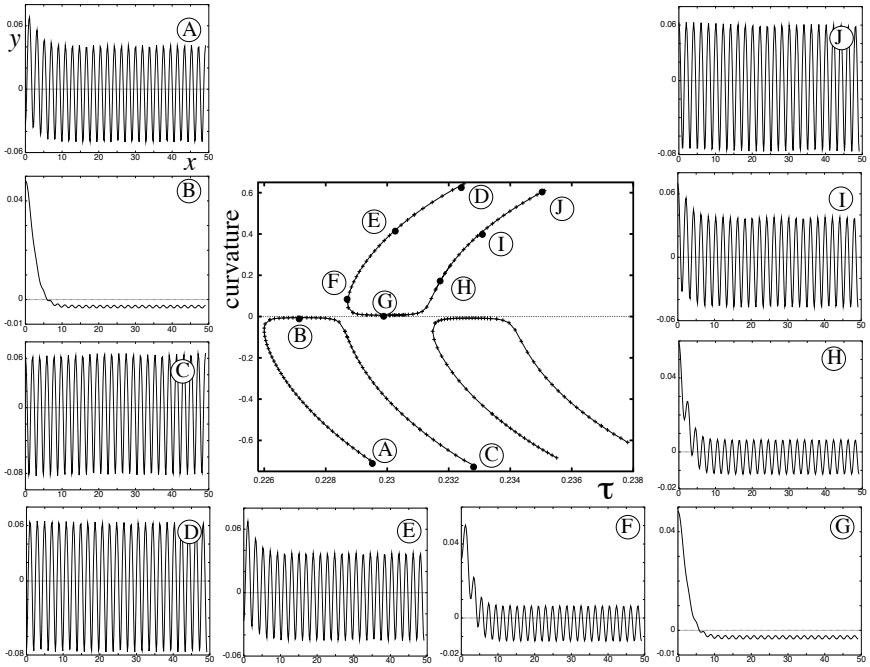

Fig. 4. Equivalent diagram to Fig. 3 for the Euler-equation formulation of water waves in the presence of surface tension plotted as Bond number τ against a signed measure of the tail amplitude for fixed Froude number $F = 1.002$ and for fixed domain size $L = 98.33$. Reproduced from A.R. Champneys, J.M. Vanden-Broeck and G.J. Lord, Do true elevation gravity-capillary solitary waves exist? a numerical investigation, *J. Fluid Mech.*, 454 (2002) 403–417 © 2002, with permission from Cambridge University Press.

to make such structures move with wave speed $c \neq 0$, they typically shed radiation and eventually stop or cease to survive as coherent structures.

Moving discrete breathers can be sought by making the substitution

$$u_n(t) = \psi(z)\mathrm{e}^{-\mathrm{i}\Lambda t} \qquad \text{with } z = n - ct \in \mathbb{R}$$

which gives the advanced-retarded equation

$$-\mathrm{i}c\psi'(z) = (2\varepsilon - \Lambda)\psi(z) - \varepsilon(\psi(z+1) + \psi(z-1)) + \frac{\psi(z)}{1+|\psi(z)|^2}, \qquad (19)$$

for which we seek homoclinic solutions $\psi(z) \to 0$ as $z \to \pm\infty$. Simple spectral analysis shows that the spectrum of the problem linearised about $\psi = 0$ is symmetric with respect to the imaginary axis, so that the dimension n^c of the centre manifold is even; moreover, $n^c \geq 2$ for all $c, \varepsilon > 0$. Counting the codimension of the stable and unstable manifolds shows that the best we can hope for is that $n^c = 2$, and then homoclinic solutions to (19) should

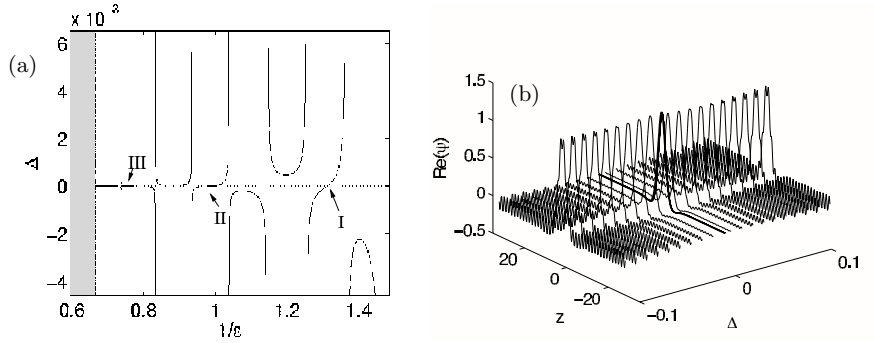

Fig. 5. Continuation of breathers on a periodic background for various values of $1/\varepsilon$ showing three zeros in δ for $c = 0.7$, $\Lambda = 0.5$, and $L = 60$ (a); the shaded region represents the spectral band where any embedded solitons would be of codimension two. Panel (b) shows solutions on the branch with zero of δ near $\varepsilon = 1.02$. Reproduced from T.R.O. Melvin, A.R. Champneys, P.G. Kevrekidis and J. Cuevas, Radiationless traveling waves in saturable nonlinear Schrödinger lattices, *Phys. Rev. Lett.* 97 (2006) 124101 © 2006, with permission from the American Physical Society.

exist along codimension-one lines in the parameter plane. An efficient way to compute such solutions is to seek solutions on a large interval $z \in [-L, L]$ with appropriate boundary conditions. Note that (19) is invariant under the reversing transformation

$$\mathcal{R}: \quad z \longrightarrow -z, \quad (\operatorname{Re}\psi, \operatorname{Im}\psi) \longrightarrow (-\operatorname{Re}\psi, \operatorname{Im}\psi).$$

We can find $\mathcal{R}$-symmetric periodic solutions by seeking solutions with $\psi(-L) \in \operatorname{Fix}(\mathcal{R})$, $\psi(0) \in \operatorname{Fix}(\mathcal{R})$. The use of these boundary conditions effectively fixes the phase symmetry $\phi \to \mathrm{e}^{\mathrm{i}g}\phi$ according the theory of Sec. 1.

An efficient way to solve such boundary-value problems is to use a pseudo-spectral method [16] by making the substitution

$$\psi(z) = \sum_{j=1}^{N} a_j \cos(\pi j z/L) + \mathrm{i} b_j \sin(\pi j z/L) \tag{20}$$

for the unknown coefficients (a_j, b_j). Substitution of (20) into (19) and evaluating at the collocation points $z_j = \frac{jL}{-2(N+1)}$ leads to a regular systems of $2N$ algebraic equations that can be solved numerically.

In particular, we can use this method to compute periodic solutions of fixed large period that approximate *quasi-solitons* made up of an exponentially localised core ψ_{core} and a non-vanishing oscillatory background ψ_{tail}:

$$\psi(z) = \psi_{\text{core}}(z) + \psi_{\text{tail}}(z).$$

At a sufficient distance from the centre of the breather ψ_{core} is zero due to its exponential localisation and, therefore, we are left with the tail which, if

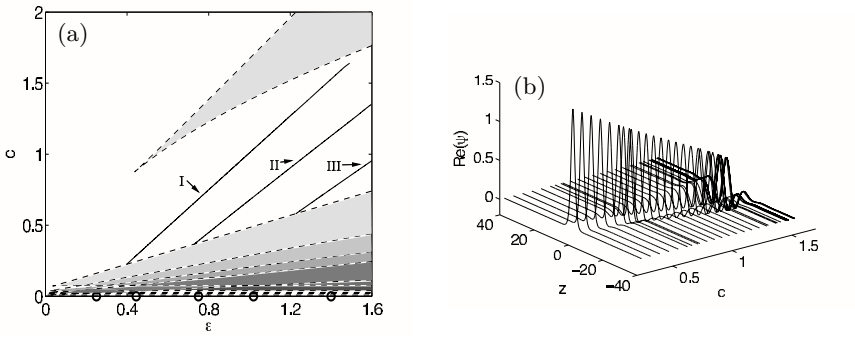

Fig. 6. Continuation of the three zeros of δ shown in Fig. 5, varying ε and c with $\Lambda = 0.5$ (a); the depth of shading represents the number of pairs $n^c/2$ of imaginary eigenvalues of the linearised problem in each parameter region: white $n^c = 2$, lightest gray $n^c = 4$, and so on; circles on the $\{c = 0\}$ axis indicate the transparent points at which the energy barrier for steady breathers vanishes. Panel (b) shows the real parts of solutions on the first branch, whose amplitude goes to zero as the upper grey wedge is approached. Reproduced from T.R.O. Melvin, A.R. Champneys, P.G. Kevrekidis and J. Cuevas, Radiationless traveling waves in saturable nonlinear Schrödinger lattices, *Phys. Rev. Lett.* 97 (2006) 124101 © 2006, with permission from the American Physical Society.

it is of small amplitude, is in the centre manifold and hence approximately sinusoidal. Because of the way $\psi(z)$ has been approximated in (20) we know that the imaginary part of $\psi_{\text{tail}}(z)$ is odd around $z = 0$ and the quantity

$$\delta = \operatorname{Im} \psi(L/2)$$

can be used as a signed measure of the amplitude of the tail. Regular zeros of δ can be followed in multiple parameters, and these give the travelling discrete breathers that we are seeking. These moving structures with zero tails were found to be remarkably stable as solutions to the initial value problem.

Figure 5 shows the results of computations of solutions with periodic tails for fixed c and Λ, but with ε allowed to vary. Note that the U- and N-shaped nature of the branches is qualitatively the same as in Fig. 4, except here we see the occasional S-shaped dislocation of the Us and Ns. These lead to values of c at which the measure Δ of the tail amplitude undergoes a regular zero. Hence, we have found a truly localised solution that can be continued in two parameters. Three such zeros are found in Fig. 5, which leads to the three branches labelled I, II and III in Fig. 6. Note that these branches terminate when they reach the boundary of the white region in Fig. 6(a), when $n^c = 2$ is no longer satisfied. More details can be found in [32].

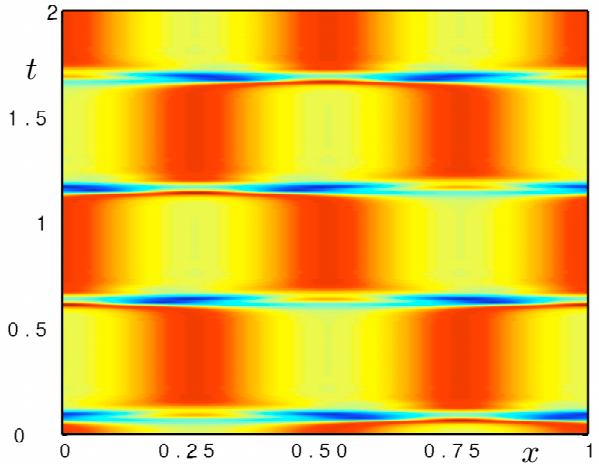

Fig. 7. A space-time contour plot of a typical heteroclinic cycle of (21) is shown for $R = 70$, $\nu = 1$, and $\mu = -4$, where dark colour corresponds to smaller and light colour to larger values of the amplitude $|u(x,t)|$. Reproduced from D.J.B. Lloyd, A.R. Champneys and R.E. Wilson, Robust heteroclinic cycles in the one-dimensional complex Ginzburg-Landau equation, *Physica D* 204 (2005) 240–268 © 2005, with permission from Elsevier Science.

5 Computing robust heteroclinic cycles

Heteroclinic cycles are formed of trajectories that connect equilibria or periodic orbits. This behaviour is typically structurally unstable in generic dynamical systems. However, in systems with symmetry robust connections between saddles can occur if each saddle is actually a sink within an invariant subspace generated by a discrete symmetry.

As an example, we consider the one-dimensional complex Ginzburg–Landau equation (CGL)

$$u_t = (1 + \mathrm{i}\nu)u_{xx} + Ru - (1 + \mathrm{i}\mu)|u|^2 u \tag{21}$$

on a periodic domain $x \in \mathbb{S}^1 \cong [0,1]/\sim$, where $u \in \mathbb{C}$ and $\nu, \mu, R \in \mathbb{R}$. The CGL (21) is invariant under the action of the $\mathbb{S}^1$ phase symmetry

$$u(x) \longmapsto \mathrm{e}^{\mathrm{i}\phi} u(x)$$

and the O(2)-symmetry

$$u(x) \longmapsto u(-x), \qquad u(x) \longmapsto u(x - y)$$

for $y \in \mathbb{S}^1 \cong [0,1]/\sim$.

A typical heteroclinic cycle of (21), obtained by a direct integration, is shown in Fig. 7. We observe long dormant behaviour followed by bursts of

spatio-temporal activity. The dormant states are relative equilibria of (21) of the form

$$u(x,t) = U(x)\mathrm{e}^{\mathrm{i}\omega t} \tag{22}$$

that are reflection symmetric about $x = 0.5$ and satisfy $U(x+1/2) = U(x)$ for all x. The relative equilibria observed in Fig. 7 are all related by a $1/4$-spatial translation. The bursts are characterised by initial symmetry breaking with spatial wavenumber $k = 2\pi$ of the relative equilibria (22), and the corresponding heteroclinic orbits lie in the fixed-point space generated by reflection across $x = 0$, $x = 1/4$, $x = 1/2$ or $x = 3/4$. The trajectory shown in Fig. 7 follows these different heteroclinic orbits seemingly randomly.

Since we have periodic boundary conditions, it is natural to use Fourier modes and, following [31], we therefore seek solutions of the form

$$u(x,t) = \mathrm{e}^{\mathrm{i}\phi(t)} \sum_{n\in\mathbb{Z}} W_n(t)\mathrm{e}^{2\pi\mathrm{i}nx} \tag{23}$$

where we choose $\phi(t)$ so that $W_0(t)$ is real-valued, while $W_n(t)$ is complex-valued for $n \neq 0$, to factor out the $\mathbb{S}^1$ phase symmetry. Substituting (23) into (21) yields the infinite-dimensional system

$$\mathrm{i}\dot{\phi}(t)W_n + \dot{W}_n = [R - (2\pi n)^2(1+\mathrm{i}\nu)]W_n - (1+\mathrm{i}\mu) \sum_{k-l+m=n} W_k\overline{W}_l W_m \tag{24}$$

which governs the evolution of W_n, where the phase velocity $\dot{\phi}$ is expressed explicitly by

$$\dot{\phi} = \mathrm{Im}\left[-\frac{1+\mathrm{i}\mu}{W_0} \sum_{k-l+m=0} W_k\overline{W}_l W_m\right]. \tag{25}$$

If we wish to compute the heteroclinic orbit in the fixed-point space of functions invariant under the reflection across $x = 0$, we would restrict ourselves to functions that are even in x and set $W_n = W_{-n}$ for all $n \in \mathbb{Z}$. This would then allow us to obtain the desired heteroclinic orbit as a codimension-zero saddle-sink connection using again a boundary-value formulation.

Instead, we now describe the results obtained in [28] for the $N = 2$ Fourier truncation of (24) without assuming any relation between W_n and W_{-n}; in particular, (24) is five-dimensional for $N = 2$. The results are shown in Fig. 8. The spatial average mode W_0, shown as a solid curve, exhibits the standard heteroclinic cycle behaviour. The quantities $\mathrm{Re}(W_{-1}-W_1)$ and $\mathrm{Re}(W_{-2}-W_2)$ measure how far we are away from the fixed-point space of even functions. We find that the quantity $\mathrm{Re}(W_{-2} - W_2)$ vanishes for all times even though $W_2, W_{-2} \neq 0$. This implies, and can be checked numerically, that $W_{-2}(t) = W_2(t)$ is a spatial symmetry of the heteroclinic cycles. The other quantity $\mathrm{Re}(W_{-1}-W_1)$ is plotted as the dashed curve in Fig. 8 and turns out to vanish for approximately half the heteroclinic connections. Hence, roughly half of the heteroclinic connections lie in the invariant subspace $\{W_{-n} = W_n;\ n \neq 0\}$

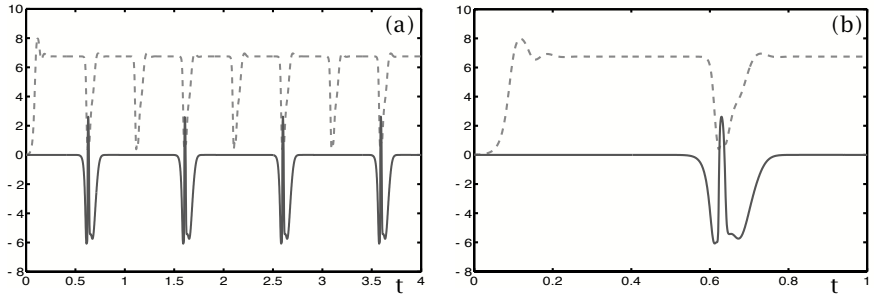

Fig. 8. Heteroclinic cycle in Fourier space (a) found by direct simulation of (24) with $N = 2$ for $R = 70$, $\mu = -4$, and $\nu = 1$; the solid curve shows the evolution of W_0, while the dashed curve gives $\mathrm{Re}(W_{-1} - W_1)$. Panel (b) shows an enlargement of the cycle. Reproduced from D.J.B. Lloyd, A.R. Champneys and R.E. Wilson, Robust heteroclinic cycles in the one-dimensional complex Ginzburg-Landau equation, *Physica D* 204 (2005) 240–268 © 2005, with permission from Elsevier Science.

corresponding to even functions. If we plotted $\mathrm{Re}(W_{-1} + W_1)$, then we would see that this quantity is also zero half of the time but for precisely the other half of heteroclinic connections. This then gives us the invariant subspace of odd functions. Both subspaces intersect at the equilibria where $W_{-1} = W_1 = 0$ allowing for structurally stable heteroclinic cycles to exist to such equilibria within either subspace.

6 Travelling waves on cylinders $\mathbb{R} \times \mathbb{S}^1$

We now treat the case of PDEs on multi-dimensional domains with a single unbounded direction. For simplicity we shall restrict to two spatial dimensions and assume periodic boundary conditions in the other direction. Rather than presenting the general theory, which can be found in [30], we treat a specific example which is concerned with localised buckling of cylindrical shells [29].

Consider an infinitely long cylinder of radius R and shell thickness t. The equilibrium for the in-plane stress function Φ and displacement w in the post-buckling regime of the cylinder is governed by the von Kármán–Donnell equations:

$$\kappa^2 \nabla^4 w + \lambda w_{xx} - \rho \phi_{xx} = w_{xx}\phi_{yy} + w_{yy}\phi_{xx} - 2w_{xy}\phi_{xy} \tag{26}$$

$$\nabla^4 \phi + \rho w_{xx} = (w_{xy})^2 - w_{xx}w_{yy}, \tag{27}$$

where ∇^4 denotes the two-dimensional bi-harmonic operator, $x \in \mathbb{R}$ is the axial and $y \in [0, 2\pi R)$ the circumferential coordinate. Furthermore, $\rho := 1/R$ is the curvature, $\kappa^2 := t^2/12(1-\nu^2)$, ν is Poisson's ratio, and the bifurcation parameter is $\lambda := P/Et$ where P is the compressive axial load (force per unit length), and E is Young's modulus. The form of solutions sought are localised

in the axial length, but circumferentially periodic, suggesting that equations (26)–(27) should be supplemented with periodic boundary conditions in y and asymptotic boundary conditions in the axial direction x. Simplifications can be made by considering two types of symmetry conditions in the mid plane of the cylinder, namely

$$\begin{aligned} \mathcal{R}: &\quad w(x,y) = w(-x,y), \quad \phi(x,y) = \phi(-x,y) \\ \mathcal{S}: &\quad w(x,y) = w(-x,y+\pi R/s), \quad \Phi(x,y) = \Phi(-x,y+\pi R/s), \end{aligned}$$

where s is the axial wavenumber of the post-buckling pattern sought.

The numerical approach taken in [29] is to use a spectral decomposition circumferentially for each value of s of the form

$$w(x,y) = \sum_{j=0}^{N} a_j(x)\cos(js\rho y), \qquad \phi(x,y) = \sum_{j=0}^{N} b_j(x)\cos(js\rho y),$$

allied to Galerkin projection, to reduce the PDEs (26)–(27) to a system of $2N$ fourth-order ODEs, each akin to (17), for the amplitudes $(a_j, b_j)(x)$. The symmetries $\mathcal{R}$ and $\mathcal{S}$ provide two different reversing transformations of the ODEs, and so the projection boundary condition at one end can be replaced by using the Fix($\mathcal{R}$) or Fix($\mathcal{S}$) boundary conditions depending on which symmetric solution is sought.

Figure 9(a) and (b) shows numerical continuation results for both $\mathcal{R}$-symmetric and $\mathcal{S}$-symmetric localised modes for a typical experimentally amenable geometry, but for different circumferential wavenumber s. The horizontal axis in these plots is the overall end-shortening implied by the deformation; see [29] for the details. The trend is the same for all solutions, namely that they bifurcate from the trivial solution subcritically (the load λ reduces sharply). They then reach a turning point with respect to λ at which point the branch would become stable in a controlled end-shortening experiment. Figure 9(c) shows an example of a localised buckle shape near such a fold.

7 Defects in oscillatory media

In the preceding section we discussed the computation of localised stationary solutions of PDEs posed on the cylinder $\mathbb{R} \times \mathbb{S}^1$. Here we illustrate that the computation of (not necessarily localised) time-periodic solutions of reaction-diffusion systems

$$u_t = \Delta u + f(u), \qquad x \in \mathbb{R},\ u \in \mathbb{R}^n \tag{28}$$

proceeds similarly. We denote the temporal frequency of a time-periodic solution by ω and use the rescaled time variable $\tau = \omega t$. Then time-periodic solutions of (28) are in one-to-one correspondence with solutions of

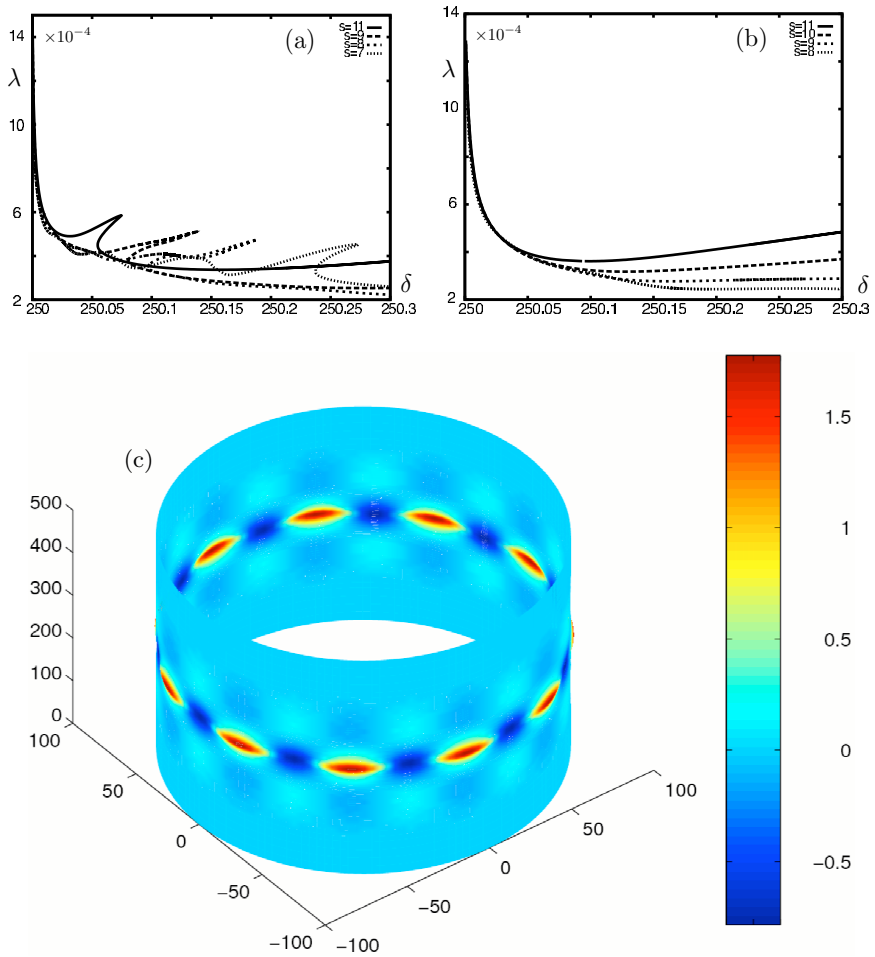

Fig. 9. Bifurcation diagrams for (a) $\mathcal{R}$-symmetric and (b) $\mathcal{S}$-symmetric solutions to (26)–(27) for different seed modes s with $\rho = 0.01$, $t = 0.247$, $\nu = 0.3$, $E = 5.56$, and $N = 6$. Panel (c) shows the displacement $w(x, y)$ of the $\mathcal{R}$-symmetric mode for $s = 11$ with λ at its local minimum value. Reproduced from G.J. Lord, A.R. Champneys and G.W. Hunt, Computation of homoclinic orbits in partial differential equations: an application to cylindrical shell buckling, *SIAM J. Sci. Comp* 21 (1999) 591–619 © 1999, with permission from the Society for Industrial and Applied Mathematics.

$$\omega u_\tau = D u_{xx} + f(u), \qquad (x, \tau) \in \mathbb{R} \times \mathbb{S}^1, \tag{29}$$

where τ is restricted to $\mathbb{S}^1 \cong [0, 2\pi]/\sim$. We now have two symmetries present in our system, namely translations in x and in t. Thus, we need to add two phase conditions, which we choose according to Remark 1, and we also need to add the generator $c\partial_x u$ of the spatial translation to (29).

We obtain the system

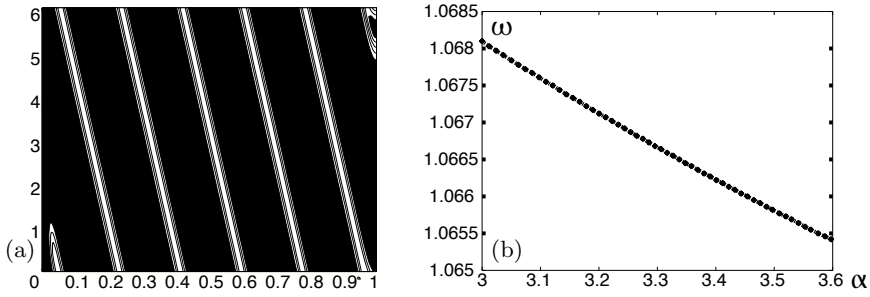

Fig. 10. The left-hand figure is a space-time contour plot of the third component $u_3(x,\tau)$ of the solution to the Rössler system [space x horizontal and rescaled time τ upwards]. Since defect is symmetric with respect to the reflection $x \mapsto -x$, the solution is plotted only for $x \geq 0$. The right-hand plot show the dependence of the temporal frequency ω on the parameter α.

$$\begin{pmatrix} -\omega u_\tau + D u_{xx} + c u_x + f(u) \\ \int_0^{2\pi} \int_{\mathbb{R}} \langle \partial_\tau u_*(x,\tau), u(x,\tau) - u_*(x,\tau) \rangle \, \mathrm{d}x \, \mathrm{d}\tau \\ \int_0^{2\pi} \int_{\mathbb{R}} \langle \partial_x u_*(x,\tau), u(x,\tau) - u_*(x,\tau) \rangle \, \mathrm{d}x \, \mathrm{d}\tau \end{pmatrix} = 0 \tag{30}$$

which we wish to solve for (u, ω, c), where u is defined on $\mathbb{R} \times \mathbb{S}^1$. In practice, one truncates the real line $\mathbb{R}$ to a large interval $(-L, L)$ and impose additional boundary conditions such as Neumann at $x = \pm L$.

As an example, we consider the three-component Rössler system with $u \in \mathbb{R}^3$ where $D = 0.4$ and

$$f(u;\alpha) = (-u_2 - u_3, u_1 + 0.2u_2, 0.2 + u_1 u_3 - \alpha u_3)^T \tag{31}$$

is the nonlinearity which depends on a parameter α. In [35], a defect solution was computed by implementing the system (30) with Neumann boundary conditions at $x = \pm L$ in AUTO [14]. The time direction τ is discretised using finite differences, taking the periodic boundary conditions for τ into account. The resulting system of ODEs in the spatial variable x is solved in AUTO as a boundary-value problem.

Note that a symmetry condition $x \to -x$ is used at the left-hand boundary in Fig. 10(a). Thus the defect is occuring along this edge of the plot. This defect solution is robust and can be continued with the algorithm outlined above. An example of such numerical compuation is shown in Fig. 10(b).

8 Localised structures in $\mathbb{R}^2$

Localised planar structures arise in many applications. Examples are light bullets in optical fibres [41], localised roll patterns known as convectons in binary-fluid convection [34], buckling modes in mechanical structures [19],

Belousov-Zhabotinhsky reaction [43], localized micro-structures in solidification [20], and oscillating localised patterns known as oscillons in vertically vibrated sand layers [17, 42].

Rather than attempting a general discussion of how these patterns could be computed numerically, we focus on localised stationary hexagonal structures in the the planar Swift–Hohenberg equation

$$[1 + \Delta]^2 u + \mu u - \nu u^2 + u^3 = 0. \tag{32}$$

Three typical localised hexagon structures are shown in Fig. 11; note that solutions (a)–(c) are computed for the same values of the parameters μ and ν. There are different ways for attempting to compute such patterns. We may, for instance, discretise in Cartesian coordinates and use three phase conditions to remove translation and rotation symmetries; see, e.g. [27]. However, a discretisation in Cartesian coordinates will give preference to patterns with D_4 symmetry, thus possibly leading to spurious solutions when computing hexagonal structures.

An alternative approach is pursued in [8] where the patterns shown in Fig. 11 were computed using polar coordinates. We now describe the latter approach in more detail. Written in polar coordinates (r, θ), the Swift–Hohenberg equation for $u(r, \theta)$ is given by

$$[1 + \Delta]^2 u + \mu u - \nu u^2 + u^3 = 0 \tag{33}$$

where

$$\Delta_{r,\theta} u = u_{rr} + \frac{1}{r} u_r + \frac{1}{r^2} u_{\theta\theta}.$$

The computational domain is $\theta \in \mathbb{S}^1 \cong [0, 2\pi]/\sim$ and $0 < r < R$ for some $R \gg 1$ with the boundary condition

$$u(R, \theta) = u_r(R, \theta) = 0, \qquad \theta \in \mathbb{S}^1 \cong [0, 2\pi]/\sim \tag{34}$$

at $r = R$.

Solutions are now sought using the Fourier ansatz

$$u(r, \theta) = \sum_{n=0}^{N-1} a_n(r) \cos(6n\theta) \tag{35}$$

which exploits the D_6-symmetry inherent to hexagons. With this ansatz, the boundary conditions (34) become

$$a_n(R) = a_n'(R) = 0, \qquad n = 0, \ldots, N-1. \tag{36}$$

We need to supplement these conditions with pole conditions at $r = 0$ to take care of the singularity of the Laplace operator at the origin. We choose to work with the pole conditions

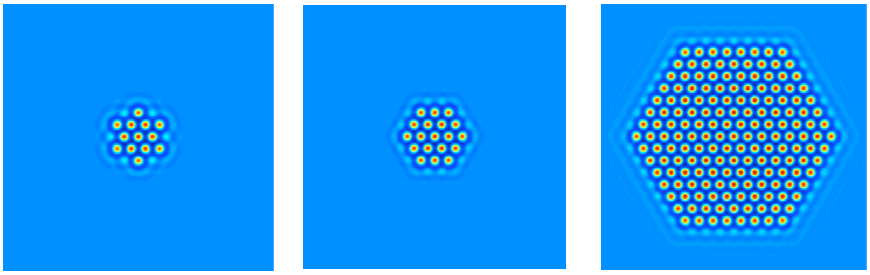

(a) (b) (c)

Fig. 11. A spatial contour plot of three localised hexagon structure (a)–(c) of the planar Swift–Hohenberg equation (32) with $\mu = 0.3$ and $\nu = 1.6$. The computational domain is $R = 100$, and $N = 20$ Fourier modes were used; plotted are the solutions on a 50×50 square.

$$a_0'(0) = a_0'''(0) = a_k(0) = a_k''(0) = 0, \qquad n = 1, \ldots, N-1 \tag{37}$$

which enforces that $u(r, \theta)$ is even in r and makes the variational formulation of (33) well defined at $r = 0$.

Figure 11 shows results of a computation where the resulting ODE boundary-value problem has been implemented and solved with AUTO. Note that localised hexagonal structures of arbitrarily wide spatial extent can be computed this way. In fact panels (a)–(c) are three hexagonal patterns on the same continuation branch; details will appear in [8].

9 Planar spiral waves

As a final example, let us comment briefly on the computation of spiral wave solutions of a planar reaction-diffusion system

$$u_t = D\Delta u + f(u), \qquad x \in \mathbb{R}^2,\ u \in \mathbb{R}^n.$$

Spiral waves are relative equilibria with respect to the rotation symmetry of the plane and, therefore, of the form $u(r, \theta, t) = u_*(r, \theta - \omega t)$ in polar coordinates (r, θ). In particular, the spiral-wave profile $u_*(r, \theta)$ is a solution to the elliptic system

$$D\Delta_{r,\theta} u + \omega \partial_\theta u + f(u) = 0. \tag{38}$$

To factor out the rotation symmetry, we may add the phase condition

$$\int_0^{2\pi} \langle \partial_\theta u_*(R/2, \theta), u(R/2, \theta) - u_*(R/2, \theta) \rangle \, \mathrm{d}\theta = 0 \tag{39}$$

posed at $r = R/2$.

Fig. 12. A contour plot of the third component u_3 of a spiral-wave solution to the planar Rössler system (28) with (31) is shown.

To solve (38)–(39), we truncate to the computational domain $(r, \theta) \in (0, R) \times [0, 2\pi]$ with periodic boundary conditions in θ and Neumann boundary conditions at $r = R$ plus appropriate pole conditions at $r = 0$. Barkley [2] then used finite differences in r and a spectral method in θ to compute spiral waves in the two-dimensional FitzHugh–Nagumo system (14).

Figure 12 shows the example of one such computation for the Rössler system (28) with (31) in two spatial dimensions, where we used Barkley's numerical code [2]. Shown is a contour plot of the third component u_3 of a spiral-wave solution at a fixed instant in time.

10 Outlook

We have attempted to outline a general approach to computing various kinds of coherent structures on infinite or semi-infinite domains. This procedure involves setting up formally well-posed boundary-value problems that factor out the symmetries or degeneracies that arise due to the particular nature of the coherent structure in question. In essence, most of our methods rely on reduction to a two-point boundary-value problem, even when solving problems in the plane. Thus, one can harness the full power of software such as AUTOfor the continuation of paths of such solutions as parameters vary.

However, to compute more general patterned states, one needs to solve boundary-value problems in appropriate two- or three-dimensional spatial domains without the artifical reduction to one-dimensional spatial problems. A reliable package for the continuation of solutions to fully two- and three-dimensional elliptic problems is clearly a pressing requirement. Such a package should be easy to use, yet sufficiently powerful. This would enable the user

to set up specific boundary conditions that factor out the symmetries, in the manner described here, in dependence on the underlying properties of the structures that are sought.

Another pressing need, and the subject of much ongoing research, is the derivation of algorithms that are able to compute information on the spectral stability of the coherent structures while these structures themselves are being computed.

Acknowledgments

We thank David Lloyd for his helpful comments and suggestions and, especially, for his help with text and figures in Secs. 5 and 8. The results reviewed here have been obtained in collaboration over many years, and we would like to thank Jesús Cuevas, Giles Hunt, Panayotis Kevrekidis, Yuri Kuznetsov, David Lloyd, Gabriel Lord, Thomas Melvin, Bart Oldeman, Arnd Scheel, Jean- Mark Vanden-Broek, and Eddie Wilson for their contributions. We are grateful to Elsevier Science, Cambridge University Press, the American Physical Society, and the Society for Industrial and Applied Mathematics for permission to reproduce previously published material.

References

1. F. S. Bai, G. J. Lord, and A. Spence. Numerical computations of connecting orbits in discrete and continuous dynamical systems. *Internat. J. Bifurc. Chaos Appl. Sci. Engrg.*, 6:1281–1293, 1996.
2. D. Barkley. Linear stability analysis of spiral waves in excitable media. *Phys. Rev. Lett.*, 68:2090–2093, 1994.
3. W.-J. Beyn. The numerical computation of connecting orbits in dynamical systems. *IMA J. Num. Anal.*, 9:379–405, 1990.
4. W.-J. Beyn. On well-posed problems for connecting orbits in dynamical systems. *Contemp. Math.*, 172:131–168, 1995.
5. W.-J. Beyn and J. M. Kleinkauf. The numerical computation of homoclinic orbits for maps. *SIAM J. Num. Anal.*, 34:1207–1236, 1997.
6. A. R. Champneys. Homoclinic orbits in reversible systems and their applications in mechanics, fluids and optics. *Physica D*, 112:158–186, 1998.
7. A. R. Champneys, Yu. A. Kuznetsov, and B. Sandstede. A numerical toolbox for homoclinic bifurcation analysis. *Internat. J. Bifur. Chaos Appl. Sci. Engrg.*, 6(5):867–887, 1996.
8. A. R. Champneys, D. J. Lloyd, and B. Sandstede. Localised patterns in the planar Swift-Hohenberg equation. in preparation.
9. A. R. Champneys and G. J. Lord. Computation of homoclinic solutions to periodic orbits in a reduced water-wave problem. *Physica D*, 102:101–124, 1997.
10. A. R. Champneys, J. M. Vanden-Broeck, and G. J. Lord Do true elevation gravity-capillary solitary waves exist? a numerical investigation. *J. Fluid Mech.*, 454:403–417, 2002.

11. C. M. deSterke and J. E. Sipe. Gap solitons. *Progr. Opt.*, 33, 1994.
12. R. L. Devaney. Reversible diffeomorphisms and flows. *Trans. Amer. Math. Soc.*, 218:89–113, 1976.
13. L. Dieci and J. Rebaza. Point-to-point and perioidic-to-periodic connections. *BIT Num. Math.*, 44:41–62, 2004.
14. E. J. Doedel, R. C. Paffenroth, A. R. Champneys, T. F. Fairgrieve, Yu. A. Kuznetsov, B. E. Oldeman, B. Sandstede, and X. Wang. AUTO2000: Continuation and bifurcation software for ordinary differential equations (with HOMCONT). Technical report, Concordia University, 2002.
15. E. J. Doedel and M. J. Friedman, Numerical computation of heteroclinic orbits. *J. Comp. Appl. Math.*, 26:317–327, 1989.
16. D. B. Duncan, J. C. Eilbeck, H. Feddersen, and J. A. D. Wattis. Solitons on lattices. *Physica D*, 68:1–11, 1993.
17. J. Fineberg. Physics in a jumping sandbox. *Nature*, 382:793–764, 1996.
18. M. J. Friedman and E. J. Doedel. Numerical computation and continuation of invariant manifolds connecting fixed points. SIAM *J. Numer. Analysis*, 28:789–808, 1991.
19. G. W. Hunt, M. A. Peletier, A. R. Champneys, P. D. Woods, M. Ahmer Wadee, C. J. Budd, and G. J. Lord. Cellular buckling in long structures. *Nonlin. Dyn.*, 21:3–29, 2000.
20. H. Jamgotchian, N. Bergeon, D. Benielle, P. Voge, B. Billia, and R. Guerin. Localised Microstructures Induced by Fluid Flow in Directional Solidification. *Phys. Rev. Lett.*, 87(16):166105, 2001.
21. J. M. Bergamin, T. Bountis, and M. N. Vrahatis. Homoclinic orbits of invertible maps. *Nonlinearity*, 15:1603–1619, 2002.
22. B. Krauskopf and T. Riess. Numerical analysis of heteroclinic connections between hyperbolic equilibria and hyperbolic periodic orbits. unpublished, 2007.
23. M. Krupa, B. Sandstede, and P. Szmolyan. Fast and slow waves in the FitzHugh–Nagumo equation. *J. Differ. Eqns.*, 133(1):49–97, 1997.
24. Yu. A. Kuznetsov. *Elements of applied bifurcation theory.* (Springer-Verlag, New York, USA, third edition, 1994).
25. Yu. A. Kuznetsov. Computation of invariant manifold bifurcations. In D. Roose, A. Spence, and B. De Dier, editors, *Continuation and Bifurcations: Numerical Techniques and Applications*, pages 183–195 (Kluwer, Dordrecht, Netherlands, 1990).
26. L. X. Liu, G. Moore, and R. D. Russell. Computation and continuation of homoclinic and heteroclinic orbits with arclength parameterization. *SIAM J. Sci. Comp.*, 18:69–93, 1997.
27. D. J. B. Lloyd and A. R. Champneys. Efficient numerical continuation and stability analysis of spatiotemporal quadratic optical solitons. *SIAM J. Sci. Comp.*, 27(3):759–773, 2005.
28. D. J. B. Lloyd, A. R. Champneys, and R. E. Wilson. Robust heteroclinic cycles in the one-dimensional complex ginzburg-landau equation. *Physica D*, 204:240–268, 2005.
29. G.J . Lord, A. R. Champneys, and G. W. Hunt. Computation of homoclinic orbits in partial differential equations: An application to cylindrical shell buckling. *SIAM J. Sci. Comp*, 21:591–619, 1999.
30. G. J . Lord, D. Peterhof, B. Sandstede, and A. Scheel. Numerical computation of solitary waves in infinite cylindrical domains. *SIAM J. Numer. Anal.*, 37(5):1420–1454, 2000.

31. B. P. Luce. Homoclinic explosions in the complex Ginzburg-Landau equation. *Physica D*, 84(3-4):553–581, 1995.
32. T. R .O. Melvin, A. R. Champneys, P. G. Kevrekidis, and J. Cuevas. Radiationless traveling waves in saturable nonlinear Schrödinger lattices. *Phys. Rev. Lett.*, 97:124101, 2006.
33. F. J. Muñoz Almaraz, E. Freire, J. Galán, E. Doedel, and A. Vanderbauwhede. Continuation of periodic orbits in conservative and hamiltonian systems. *Physica D*, 181:1–38, 2003.
34. J. J. Niemela, G. Ahlers, and D. S. Cannell. Localised travelling-wave states in Binary-Fluid convection. *Phys. Rev. Lett.*, 1990.
35. B. E. Oldeman and B. Sandstede. Numerical computation of defects in the Rössler model. unpublished.
36. B. E. Oldeman, B. Krauskopf, and A. R. Champneys. Death of period-doublings: locating the homoclinic-doubling cascade. *Physica D*, 146:100–120, 2000.
37. A. J. Rodríguez-Luis, E. Freire, and E. Ponce. A method for homoclinic and heteroclinic continuation in two and three dimensions. In D. Roose, A. Spence, and B. De Dier, editors, *Continuation and Bifurcations: Numerical Techniques and Applications*, pages 197–210 (Kluwer, Dordrecht, Netherlands, 1990).
38. B. Sandstede. Convergence estimates for the numerical approximation of homoclinic solutions. *IMA J. Num. Anal.*, 17:437–462, 1997.
39. C. Sparrow. *Lorenz Equations : Bifurcations, Chaos, and Strange Attractors.* (Springer-Verlag, New York, 1982).
40. S. M. Sun. Non-existence of truly solitary waves in water with small surface tension. *Proc. Royal Soc. A*, 455(1986):2191–2228, 1999.
41. M. Tlidi, A. G. Vladimirov, and P. Mandel. Interaction and stability of periodic and localised structures in optical bistable systems. *IEEE J. of Quant. Electr.*, 39(2):216–226, 2003.
42. P. B. Umbanhowar, F. Melo, and H. L. Swinney. Localised excitations in a vertically vibrated granular layer. *Nature*, 1996.
43. V. K. Vanag and I. R. Epstein. Stationary and oscillatory localised patterns, and subcritical bifurcations. *Phys. Rev. Lett.*, 92(12):128301, 2004.
44. K. Yagasaki. Numerical detection and continuation of homoclinic points and their bifurcations for maps and periodically forced systems. *Internat. J. Bifurc. Chaos Appl. Sci. Engrg.*, 8:1617–1627, 1998.
45. J. Yang, B. A. Malomed, D. J. Kaup, and A. R. Champneys. Embedded solitons: a new type of solitary wave. *Math. Comp. Simulation*, 55:585–600, 2001.